Songklanakarin J. Sci. Technol.
44 (5), 1345–1352, Sep. – Oct. 2022

http://www.sjst.psu.ac.th

Original Article

Antibacterial efficiency enhancement of gentamicin sulfate encapsulated CuS nanoparticles

Padikkamannil Abishad[1, 2], Namratha Keerthiraj[3], Srinath B. S.[2], Jayashankar Madayya[2], Jess Vergis[4], and Byrappa Kullaiya[5*]

[1] *Center for Material Science and Technology, University of Mysore, Mysuru, Karnataka, 570005 India*

[2] *Department of Studies and Research in Microbiology, Mangalore University, Mangaluru, Karnataka, 574199 India*

[3] *Centre for Advanced Studies in Precambrian Geology, Mysore, Karnataka 570006 India*

[4] *Department of Veterinary Public Health, College of Veterinary and Animal Sciences, Kerala Veterinary and Animal Sciences University, Pookode, Wayanad, 673576 India*

[5] *Centre for Research and Innovations, BGS Institute of Technology, Adichunchanagiri University, Nagara, Mandya, Karnataka, 571448 India*

Received: 6 June 2022; Revised: 10 August 2022; Accepted: 13 September 2022

Abstract

The use of engineered semiconductor nanomaterials to address multi-drug resistance in bacteria has gained attention. In this study, an environmentally friendly cost-effective biological approach to synthesize copper sulfide nanoparticles (CuS-NPs) is reported. The CuS-NPs and the antibiotic Gentamicin Sulfate (GS) at the concentration of 40 µg/mL exhibit significant synergistic inhibition against several human pathogens (*E. coli*, *Salmonella* typhi, *Klebsiella pneumoniae*, *Staphylococcus aureus*, and *Bacillus subtilis*). The effective release of antibiotic and less frequent administration are therapeutic advantages. The drug entrapment and loading capacity of synthesized CuS nanoparticles (CuS-NP) were recorded as 61% and 39%, respectively. Additionally, a promising activity of the mycosynthesized CuS-NP is an increased cytotoxicity against MDA-MB-231 breast cancer cell line, as indicated by the estimated IC50 value.

Keywords: gentamicin sulfate, CuS nanoparticles, myconanotechnology, biosynthesis, cytotoxicity

1. Introduction

Gentamicin belongs to the aminoglycoside group of antibiotics, which is commonly employed to treat a variety of bacterial infections of bones, meninges, urinary tract, as well as conditions like sepsis and pelvic inflammatory disease. Moreover, it is considered a first-line aminoglycoside candidate to treat several pathogenic microbes such as *Proteus vulgaris*, *Pseudomonas aeruginosa*, *Escherichia coli*, *Enterobacter aerogenes*, *Klebsiella pneumoniae*, and *Staphylococcus aureus* (Dorati *et al.*, 2018). Of late, antimicrobial resistance (AMR) has emerged as a global public health threat and is regarded as an evolutionary process that often arises due to the indiscriminate use of antibiotics in both human clinical and veterinary practices. Generally, the misuse and overuse of antibiotics have led to the development

*Corresponding author
Email address: kbyrappa@gmail.com

of drug resistance among bacterial pathogens, which results in a serious public health concern in treating infections of bacterial origin (Abishad *et al.*, 2021; Chen *et al.*, 2014). Additionally, the emergence of AMR has recently been associated widely to the impaired efflux pumps and genetic modifications of suitable enzymes that would reduce the efficacy of antimicrobials against bacterial agents (Luthra, Rominski & Sander, 2018).

Generally, antibiotics have a short half-life and the levels of antibiotic concentration at target sites may fluctuate. The desired concentration of an antibiotic would be attained at the site of infection by use of effective drug delivery systems. Nanotechnology-mediated delivery system offers a promising approach for restoring and enhancing the effectiveness of conventional antibiotics, by providing intra-cellular drug targeting and sustained release into the targeted cells (Dorati *et al.*, 2018). The nanoparticle (NP) based drug delivery systems could improve the bioavailability of antibiotics, which would further enhance therapeutic efficacy (Imbuluzqueta *et al.* 2013). Of late, hollow copper sulphide (CuS) NPs have been widely employed as effective antibiotic delivery vehicles (~55 nm diameter) through transdermal drug delivery using thermal ablation (Goel, Chen & Cai, 2014). For such nanoparticles, silver, gold, copper, and zinc are often used metals in the biomedical field (Kanagamani *et al.*, 2019). The biological features of copper-based transition metal nanoparticles, in particular, make them especially appropriate for use against human pathogens (Pugazhendhi *et al.*, 2018). Nanoparticles are frequently used as antibiotic alternatives because of their distinctive physicochemical characteristics, targeted delivery, and low risk of resistance development (Abishad *et al.*, 2022). Against MDR infections, tobramycine-stabilized silver nanoparticles can function as an efficient antibacterial agent (Junejo *et al.*, 2019). The synthesis of CuS NPs can be achieved either by hydrothermal (Byrappa & Adschiri, 2007), solvothermal(Zare *et al.*, 2018) or biological approach (Abishad *et al.*, 2022). While the former techniques (hydrothermal as well as solvothermal) utilize high temperature, pressure, and toxic chemicals such as hydrogen sulphide in the synthesis of CuS NPs, the latter biological approach could avoid such inconveniences. Among the various methods for biological synthesis, mycosynthesis that is fungi mediated exhibits elevated metal bioaccumulation ability and tolerance that could be beneficial for the biosynthesis of CuS NPs (Mukhopadhyay & Sarkar, 2006).

Although the fungi mediated biosynthesis can be considered an ideal approach for the synthesis of CuS NPs, the exact underlying antimicrobial mechanism of CuS NPs has not fully been revealed. The fungal cells produce extracellular enzymes and secondary metabolites, which could accelerate the biosynthesis of NPs (Guilger *et al.*, 2017). Moreover, the extracellular synthesis of CuS NPs was reported from the copper ore mine wastewater while employing the fungus *Fusarium oxysporum* for the removal of a high load of copper metal contaminants (Díez-martínez, García-fernández & Manzano, 2016; Dorati *et al.*, 2018). The present study was carried out with an objective to synthesize, characterize, and evaluate the antibacterial potential of CuS NPs employing the fungal cell mass of *Trichoderma harzianum* (biocontrol pest). Further, gentamicin was loaded into the green synthesized CuS NPs in order to assess the potential enhancement of its antibacterial activity.

2. Materials and Methods

2.1 Microorganisms and chemicals

The standard bacterial strains of *S. aureus* (MTCC 6908), *Salmonella* Typhi (MTCC 733), *K. pneumoniae* (MTCC 661), *Bacillus subtilis* (MTCC 121) and *E. coli* (MTCC 1698) were procured from the Microbial Type Culture Collection Center and Gene Bank, IMTECH, Chandigarh, India. The chemicals $CuSO_4.3H_2O$ (99.99%), gentamicin sulfate (GS), methanol and isopropanol (Fisher, UK), nutrient agar media, potato dextrose (PD) agar, RBC diluting buffer, and glutaraldehyde (HiMedia, India) were used in the present work.

The fungal culture of *T. harzianum* obtained from the Kerala Agricultural University, India, was employed in this study for the biosynthesis of CuS NPs. An initial concentration of the fungal culture (0.15 mg/mL) inoculated onto the PD agar medium was incubated at 25 to 28°C for 6 days to observe the formation of emergent mycelia. The morphological characteristics were determined in microscopic examination to confirm the fungal culture.

2.2 Mycosynthesis of CuS NPs

The fungal cultures of *T. harzianum* grown in Erlenmeyer flasks containing PD broth media (150 mL) were incubated at 25 to 28°C under shaking (200 rpm) for 6 days, before use in experiments. Subsequent to the culturing, the fungal mycelia were removed from the media by centrifugation (6000 rpm for 10 min at 5°C); the settled mycelia were washed twice in sterile nanopure water. Later, the harvested fungal cell mass (5 g) was dispersed in sterile nanopure water (50 ml) and kept in Erlenmeyer flasks at pH 5.0-6.0. To this suspension, aqueous solutions of copper sulphate at various concentrations (1 mM, 2 mM, 5 mM and 10 mM) were added and incubated at 25°C - 28°C at 180 rpm and the synthesis of CuS NPs was carried out for a period of 36 h.

2.3 Characterization of CuS NPs

The CuS NPs obtained were further characterized by UV-Vis spectroscopy, Fourier transform infrared spectroscopy (FTIR), dynamic light scattering (DLS), thermogravimetric analysis (TGA) and differential thermal analysis (DTA), powder X-ray diffraction (PXRD), atomic force microscopy (AFM), as well as scanning electron microscopy (SEM).

The obtained CuS NPs were dissolved in ultrapure water (1 mg/ml) and scanned between 250 and 750 nm to determine the UV-Vis spectra (SA-165, Elico, India). Besides, the CuS NPs were freeze dried to identify the unknown functional groups by FTIR analysis (JASCO FTIR- 460 Plus Spectrophotometer, Japan) of potassium bromide wafers at room temperature in the range 400-4000 cm^{-1}. The size distributions of the mycosynthesised CuS NPs were estimated by dynamic light scattering (BIC 90 Plus, Brookhaven Instruments Corp., USA) performed at an angle of 90º at 25°C. The TGA-DTA of CuS NPs was then recorded by heating around 18 mg samples in nitrogen atmosphere at a rate of 30°C per min in the range from 50 to 900°C (NETZSCH

STA 2500, Germany).

In order to assess the crystalline structure of the biosynthesized CuS NPs, PXRD analysis (Rigaku Smart Lab, Japan), was performed by CuKα radiation using 40 keV and 30 mA with a scanning step size of 0.02°and λ=1.544Å. Additionally, the surface texture of biosynthesized CuS NPs was studied using AFM (APE Research, Italy). Further, the morphology of CuS NPs was evaluated by examining the samples using SEM (JEOL JSM-6610 LV, Japan).

2.4 *In vitro* cytotoxicity assay

The effect of CuS NPs on the cell viability was estimated by *in vitro* MTT cytotoxicity assay (Mosmann., 1983). Briefly, the MDA-MB-231 epithelial cell line (1×10^5 cells per ml; 100 µl per well) was seeded in a 96 well plate, with replicates. Later, the cells were treated with varied concentrations (0, 5, 10, 25, 50, 100 µg/ml) of CuS NPs for 24 and 48 h. Subsequent to the incubation, MTT stock solution (5 mg/ml; 20 µl) was added to each well and incubated at 37ºC for 4 h. The formazan crystals thus obtained were solubilized with dimethyl sulfoxide (DMSO) and the absorbance was measured at 570 nm using a microplate reader (BioRad, USA) to determine the cell viability. The cell viability (expressed in %) was calculated as cell viability= (Absorbance of treated cell / Absorbance of control cells) × 100.

2.5 SEM imaging of CuS treated bacteria

The SEM imaging was performed to visualize the morphological changes of *B. subtilis* strains (taken as representative) treated with CuS NPs (80 µg/mL) for 60 min. The overnight fixed bacterial cells (2% glutaraldehyde) on clean grease-free glass coverslips were dehydrated (ethanol) and visualized by electron microscopy (JEOL JSM-6610 LV SEM, Japan).

2.6 Preparation of GS- laden CuS NPs

The aminoglycoside antibiotic GS was loaded into the mycosynthesised CuS-NPs. Briefly, CuS NPs (7 mg) was added to nanopure water (10 ml) and the mixture was stirred mildly at 400 rpm for 5 min. Subsequently, GS (16 mg) added into this mixture was stirred at 1,400 rpm for 2 h to form the GS loaded CuS NPs; the mixture was maintained for 5 min. Finally, the suspension was centrifuged (Eppendorf AG 5810R, Germany) at 12,000 rpm for 10 min to separate the nanoparticles.

The physical stability of lyophilized GS-loaded CuS NPs was examined, the optimized formulation was freeze-dried (Hawarch Scientific, China) in the presence of sucrose (0.10% w/v) as a cryoprotectant for 48 h at 0.05 mm Hg pressure. The freeze-dried samples stored at room temperature (at 25°C) were then redispersed by vortex mixing with 10 ml of ultra-pure water.

2.7 Drug loading and entrapment efficiency

The amount of GS entrapped in the CuS NPs was determined as described earlier (Chen *et al.*, 2014), with slight modifications. The GS loaded CuS NPs were centrifuged at 10,000 rpm for 30 mins, and the supernatant was collected. The bicinchoninic acid (BCA) protein estimation assay was employed to determine the concentration of GS present in the supernatant, thus providing the mass of protein remaining unencapsulated. A mass balance was performed to determine the amount of GS that was loaded into the microspheres. The loading capacity (LC; in %) of GS on CuS NPs was calculated as (Entrapped drug /nanoparticle weight) × 100.

The protein that was lost while washing the microspheres during fabrication process could not be considered while calculating the LE; hence, the LE would be slightly overestimated. The entrapment efficiency (EE; in %) of the protein was therefore determined as [(drug added-free unentrapped drug)/nanoparticle weight] × 100

2.8 *In vitro* haemolytic assay

The *in vitro* haemolytic assay of GS loaded CuS NPs was performed using chicken RBCs (Abishad et al 2022). Briefly, the freshly collected aseptic chicken blood was centrifuged at 3,000 rpm for 5 min, and the erythrocyte pellet obtained was washed four times with sterile normal saline (0.85%) solution. Subsequent to the repeated washing, sterile PBS was added to the erythrocyte pellet so as to obtain 10% suspension of chicken RBCs. Later, the haemolytic activity of the GS loaded CuS NPs (100 µg/mL) was assessed by estimating the absorbance of supernatant at 543 nm (Beckman Coulter DU 730, USA), keeping Triton-X 100 (0.10%) as the positive control.

2.9 *In vitro* antibacterial activity

With the aim to evaluate the synergistic effect of the antibiotic GS with the mycosynthesised CuS NPs, *in vitro* antibacterial assay was performed against both Gram-negative (*K. pneumonia*, *S.* Typhi and *E. coli*) as well as Gram-positive (*S. aureus*, and *B. subtilis*) bacteria in a well diffusion assay. The sterile pre-warmed Muller Hinton agar plates seeded with the test bacterial suspension (1×10^6 CFU) were treated with different concentrations of GS alone (30 µg), CuS NPs (80 µg/mL) and GS loaded CuS NPs (80 µg/mL; 40 µg/mL). All the treated plates were incubated at 37ºC for 24 h and the zone of inhibition (in mm) was measured.

3. Results and Discussion

3.1 Mycosynthesis of CuS NPs

As part of this study, the extract of *T. harzianum* reduced the aqueous solution of 2 mM copper sulphate (at a ratio of 1:4) to CuS NPs, upon incubation at 25°C under constant stirring (180 rpm) for 36 h (Figure 1a). The biocontrol fungus, *T. harzianum* was earlier used for the extracellular biosynthesis of silver NPs, in order to control an agricultural fungal infection, the white mold (Guilger *et al.*, 2017). The formation of light green colored precipitate at the bottom of the conical flask in our study (Figure 1a) indicated the biosynthesis of CuS NPs (Solanki, Sengupta, & Murthy, 2010). The biosynthesis of CuS NPs employing the fungal biomass could possibly be due to the extracellular reduction of the copper ions in the copper sulphate solution forming nucleation, followed by accumulation and stabilization of CuS

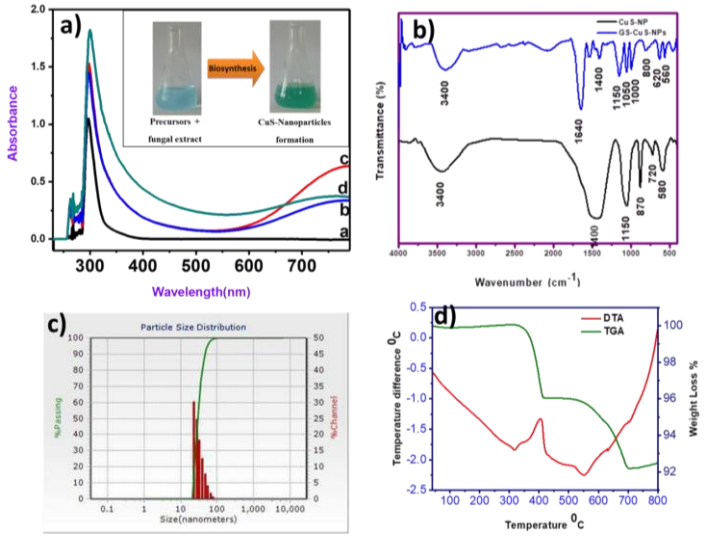

Figure 1. (a): UV-Vis spectra of CuS NPs prepared using 1mM (a), 2 mM(b), 5mM (c) and 10 mM (d) hydrated $CuSO_4$ and *T. harzianum*; (b) FTIR spectra of CuS NPs and GS-laden CuS NPs; (c) Particle size distribution of biosynthesized CuS NPs; (d) TGA/DTA curve of biosynthesized CuS NPs

NPs, depending on various factors such as concentration of copper sulphate solution, reaction time and temperature (Mukherjee *et al.*, 2001). Even though different concentrations of copper sulphate solution (1 mM, 2 mM, 5 mM and 10 mM) were employed in this study for the biological synthesis of CuS NPs, 2 mM was found to be optimal, based on the antibacterial activity on MH agar plates (data not shown). Moreover, the optimum ratio of fungal extract to copper sulphate solution for inducing the green synthesis of CuS NPs in this study was observed to be 1:4 (data not shown). Further, while employing the mycosynthesis of CuS NPs at various temperatures (25°C, 50°C, and 70°C), a reaction temperature of 25°C was observed to be optimal.

Antimicrobial resistance (AMR) is emerging as a global public health threat. With the tapered pipeline of antibiotic discovery, research has now been focussed on alternatives of antimicrobials. In recent times, nanotechnology has gained momentum in diverse fields such as antimicrobial and chemotherapeutic agents, drug delivery systems, photothermal therapy, and biosensors. Owing to its high specific surface area to volume ratio, and anti-bactericidal activity, the CuS NPs have been widely studied as effective nanomaterials in the fields of water treatment, antimicrobial food packaging, and various biomedical applications (Anvar, Ahari, & Ataee, 2021). However, the biosynthesis of CuS NPs using fungal agents has not been widely employed, barring a few studies (Mukherjee *et al.*, 2001). Moreover, this appears to be the first study of its kind on the biosynthesis of CuS NPs employing the biocontrol fungi, *T. harzianum*.

3.2 Characterization of CuS NPs

First of all, the biosynthesized CuS NPs were characterized optically by using UV-Vis spectrophotometer for analyzing the surface plasmon resonance (SPR). The suspension of CuS NPs in nanopure water exhibited a maximum absorbance at 560 nm (Figure 1a).

The FTIR analysis of CuS NPs (Figure 1b) permits spectrometric observations within the range of 400-4000 cm^{-1}. Moreover, the FTIR spectrum revealed characteristic bands corresponding to functional groups of biosynthesized CuS NPs. The spectrum observed between 500-600 cm^{-1} (Cu-S stretching mode) corresponds to the copper sulphide crystals, while at 1150 cm^{-1}, 1400 cm^{-1}, and 3400 cm^{-1} it corresponds to the characteristic C-O stretching vibrations, C-H stretching vibrations, and presence of OH functional groups, respectively (Figure 1b) (Saranya, Santhosh, Ramachandran & Grace, 2014)(Wang *et al.*, 2020). Meanwhile, the size distribution and surface charge of biosynthesized CuS NPs was recorded by DLS. The average size of CuS NPs ranged from 40 to 90 nm, while the surface charge was observed to be -200 mV (Figure 1c). In this study, the mycosynthesis of CuS NPs resulted in highly monodisperse nanoparticles with size range from 40 to 90 nm, as reported earlier (Luthra *et al.*, 2018).

To ascertain the thermal stability and thermal degradation of biologically generated NPs under continuous heating, thermogravimetric analysis (TGA) was carried out. The TGA data obtained in the present study revealed that thermal decomposition of CuS NPs started around 320°C supported by the DTA with narrow endothermic dip at 320°C and the decomposition continued till 430°C. Moreover, a weight loss of 5% up to 430°C in TGA corresponded with a sharp intense exothermic peak in DTA observed at 430°C (Figure 1d). Further, a progressive thermal degradation of the biosynthesized CuS NPs were observed from 500°C that corresponded to a narrow endothermic peak (Figure 1d). In short, the results of TGA/ DTA indicate that thermal decomposition and crystallization of the sample occurred simultaneously, which is suggestive of thermal stability.

Further, the microscopic surface morphology and topographic information of CuS NPs was assessed in AFM analysis. In the present study, quantitative measurement of surface features such as two- and three-dimensional AFM topological images of CuS NPs was done (Figure 2a; 2b). It

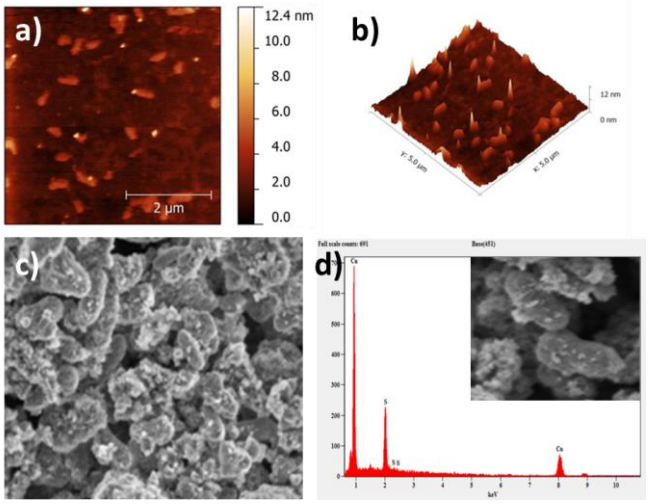

Figure 2. Surface topology and electron microscopic imaging of biosynthesized CuS NPs. AFM imaging (a; b) of CuS NPs; SEM imaging (c) of CuS NPs; and elemental analysis (d) of biosynthesized CuS NPs

was estimated that the roughness average (*R*a) and root mean square roughness (*R*q) for the mycosynthesised CuS NPs were 0.57 nm and 0.79 nm. Besides, the present study indicated the presence of comparatively lesser dents and irregularities in the surface morphology of CuS NPs (Figure 1a; 1b), which is in contradiction with an earlier report (Ajibade & Botha, 2017), with higher *R*a and *R*q values.

The morphology and microstructure of the biosynthesized CuS NPs were visualized using SEM. The SEM imaging of CuS NPs, in this study, revealed rod to spherical shapes (Figure 2c). The results of elemental analysis by energy dispersive x-ray (EDX) indicated the presence of copper and sulfur (Figure 2d). The additional peaks visualized in the EDX spectra represent stabilizing agents that originated from the fungal extract (Ottoni *et al.*, 2017).

The PXRD pattern of CuS NPs shown as Figure 3a exhibited planes at (022), (023) and (130) indexed to orthogonal structure (JCPDS Card No. 65-7111) (Qi, Wen, Wang, Jin & Zhou., 2020).

3.3 *In vitro* cytotoxicity assay

The mycosynthesised CuS NPs were subjected to *in vitro* MTT cell line based cytotoxicity assay as an indicator of cell viability and proliferation (Mosmann., 1983); (Van-Tonder, Joubert & Cromarty, 2015). In the present study, the breast epithelial MDA-MB-231 cell line was employed to estimate the half-maximal inhibitory concentration (IC_{50}) of the CuS NPs. The degree of cell viability decreased progressively with concentration of mycosynthesised CuS NPs (Figure 3b). Further, the IC_{50} of CuS NPs determined in this study was 165 µg/mL. The results of this study indicate that the mycosynthesised CuS NPs were relatively nontoxic to the epithelial cell line tested, as reported in earlier studies (Feng *et al.*, 2015)(Wang *et al.*, 2016). CuS nanoparticles have been reported to be 95% cytotoxic to Hela, SKOV3, and KB cells when incubated for a day at a concentration of 200 g/mL (Neelgund *et al.*, 2021). CuS nanoparticles exhibit toxicity at 400 g/mL concentration in 24 hours of exposure leaving 41.5 % viable cells, while being nontoxic to Hela cells at low concentrations (less than 50 g/mL) (Feng *et al.*, 2015; Mofokeng, Moloto, Shumbula & Tetyana, 2019). Extensive research has been done on the molecular mechanisms underlying nanoparticle cytotoxicity, including interactions between nanoparticles and cell surfaces that result in membrane damage or internal signaling pathway activation, the release of toxic ions from the nanoparticles that affect cell cytotoxicity, and the generation of reactive oxygen species that can cause oxidative stress and cell damage (Buchman *et al.*, 2019).

3.4 SEM imaging of CuS treated bacteria

The fixed SEM-based visualization of *B. subtilis* (taken as a representative bacterial strain) treated with CuS NPs was carried out to observe the morphological changes, along with untreated bacterial control (Figure 3c; 3d).

In this study, the SEM imaging revealed that the CuS NPs did not penetrate the bacterial cells, which could be due to the comparatively large size of CuS NPs (40 to 90 nm) relative to the pores in the cell wall of Gram-positive bacteria (4-16 nm) (Pajerski *et al.*, 2019). However, *B. subtilis*'es structural integrity is considerably altered by nanoparticle damage at specific places, which results in the loss of structural support and an irregular bacterial form. Such a scenario will cause intracellular disintegration and the loss of cytoplasmic content (Fanny Chiat Orou *et al.*, 2018).

3.5 GS-laden CuS NPs

To enhance the activity of biosynthesized CuS NPs, a broad-spectrum aminoglycoside antibiotic (GS) was used in this study. In general, GS inhibits the bacterial protein synthesis by binding to 30S ribosomal subunit and exerts bactericidal action (Papich, 2016). The antibiotic GS was conjugated to the already synthesized CuS NPs (Imbuluzqueta *et al.*, 2013) resulting in the formation of light greenish colored powder, indicating the entrapment of GS onto CuS NPs.

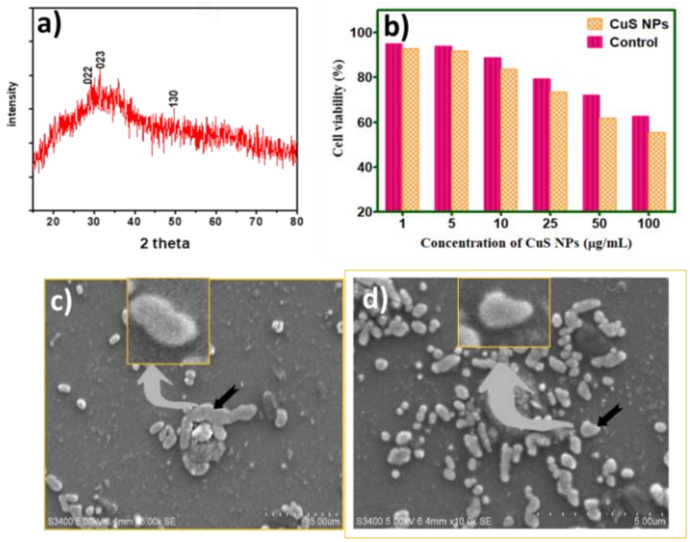

Figure 3. XRD pattern (a) of CuS NPs; MDA-MB-231 cell line based viability assay (b) of CuS-NPs; SEM micrograph of CuS NPs untreated (c) and treated (d) B. subtilis, respectively.

The GS-laden CuS NPs thus synthesized were characterized by FTIR spectroscopy (Figure 1b). On analyzing, the FTIR spectrum of GS-laden CuS NPs had a short peak at 1,400 cm^{-1} due to -NH_2 group, while the peaks observed at 1,050 cm^{-1} and 1,150 cm^{-1} for the GS-laden CuS NPs correspond to C-O stretching vibrations. Moreover, the vibrations noticed at 560 cm^{-1} could be due to the presence of metal sulphide, whereas 3,400 cm^{-1} corresponds to O-H stretching. Besides, the FTIR spectra had peaks at 1,640 cm^{-1} and 1,530 cm^{-1} corresponding to the -NH groups in Gentamicin (Figure 1b) (Dizaj *et al.*, 2015).

The application of CuS NPs as nano-carriers was assessed by estimating the drug loading as well as entrapment efficiency. In the present study, the drug loading capacity and entrapment efficiency of the mycosynthesised CuS NPs were recorded as 39% and 61%, respectively. The findings of our study indicate that the mycosynthesised CuS NPs act as better vehicles for drug loading and entrapment of GS than in an earlier study, which reported the loading of GS onto calcium carbonate NPs, wherein drug loading and entrapment efficiency were found to be 25.30% and 38.60%, respectively (Maleki Dizaj, Lotfipour, Barzegar-Jalali, Zarrintan & Adibkia, 2016).

3.6 *In vitro* haemolytic assay

The erythrocyte-mediated haemolytic assay of GS-loaded CuS NPs was employed to assess the initial toxicity. The erythrocyte is often employed as a model of host cell membrane to estimate the haemolytic activity in a rapid assessment of initial toxicity of antimicrobial agents. We employed chicken erythrocytes for determining the *in vitro* toxicity of GS-laden CuS NPs (100 µg/mL). A minimal haemolysis (5.05%) was observed for the GS-laden CuS NPs in this assay based toxicity profile (Zare *et al.*, 2018).

3.7 *In vitro* antibacterial activity

An agar well diffusion method was employed to ensure the antibacterial activity of GS-laden CuS NPs in comparison with GS alone and CuS NPs against Gram negative as well as Gram positive bacterial pathogens.

From Table 1, it can be observed that GS-laden CuS NPs (80 g/mL) inhibited the growth of tested bacterial strains more effectively than free GS and CuS NPs, based on the zone of inhibition. It is interesting to note that the loaded of GS with the CuS NPs had enhanced antibacterial activity. The pronounced *in vitro* antibacterial activity of GS-laden CuS NPs (80 µg/mL) relative to the GS-laden CuS NPs (40 µg/mL) might be due to the concentration-dependence characteristic of aminoglycoside class of antibiotics (Imbuluzqueta *et al.*, 2013)(Kotian, Abishad, Byrappa & Rai, 2019).

4. Conclusions

The CuS NPs were synthesized and characterized employing the fungal cell mass of biocontrol pest, *T. harzianum*. Later, gentamicin was loaded into the mycosynthesised CuS NPs in order to assess potential

Table 1. *In vitro* antibacterial efficacy (measured as zone of inhibition, mm) of mycosynthesised CuS NPs, GS and GS-laden CuS NPs

Candidate treatments	*E. coli*	*S.* Typhi	*K. pneumoniae*	*S. aureus*	*B. subtilis*
GS (30 µg/mL)	21±1	30±1	22±1	31±1	26±1
CuS NPs (0 µg/mL)	13±1	15±1	15±1	16±1	14±1
GS- laden CuS NPs (80 µg/mL)	25±1	27±1	27±1	33±1	29±1
GS- laden CuS NPs (40 µg/mL)	19±1	21±1	20±1	25±1	22±1

enhancement of its antibacterial activity. We observed a synergistic antibacterial efficacy of GS-laden CuS NPs against the pathogens tested. In short, the GS-laden CuS NPs were found to be effective candidates to combat pathogenic microorganisms. Moreover, the green synthesized CuS NPs as well as GS-laden CuS NPs in this study were found to be non-toxic towards the tested epithelial cell line. This study highlights an eco-friendly synthesis of semiconductor nanomaterials as potential drug carriers and opens the feasibility of biocompatible materials for drug loading in the field of nanomedicine.

Acknowledgements

This work was financially supported by the funding received from University Grants Commission, India, under University with Potential for Excellence Program (UPE), University of Mysore, Karnataka.

References

Abishad, P., Niveditha, P., Unni, V., Vergis, J., Kurkure, N. V., Chaudhari, S., . . . Barbuddhe, S. B. (2021). In silico molecular docking and in vitro antimicrobial efficacy of phytochemicals against multi-drug-resistant enteroaggregative Escherichia coli and non-typhoidal Salmonella spp. *Gut Pathogens*, *13*(1), 1–11. Retrieved from https://doi.org/10.1186/s13099-021-00443-3

Abishad, P., Vergis, J., Unni, V., Ram, V. P., Niveditha, P., Yasur, J., . . . Rawool, D. B. (2022). Green Synthesized silver nanoparticles using lactobacillus acidophilus as an antioxidant, antimicrobial, and antibiofilm agent against multi-drug resistant enteroaggregative escherichia coli. *Probiotics and Antimicrobial Proteins*. Retrieved from https://doi.org/10.1007/s12602-022-09961-1

Ajibade, P., & Botha, N. (2017). Synthesis, optical and structural properties of copper sulfide nanocrystals from single molecule precursors. *Nanomaterials*, *7*(2), 32. Retrieved from https://doi.org/10.3390/nano7020032

Anvar, A. A., Ahari, H., & Ataee, M. (2021). Antimicrobial Properties of food nanopackaging: A new focus on foodborne pathogens. *Frontiers in Microbiology*, *12*(July). Retrieved from https://doi.org/10.3389/fmicb.2021.690706

Buchman, J. T., Hudson-Smith, N. V., Landy, K. M., & Haynes, C. L. (2019). Understanding nanoparticle toxicity mechanisms to inform redesign strategies to reduce environmental impact. *Accounts of Chemical Research*, *52*(6), 1632–1642. Retrieved from https://doi.org/10.1021/acs.accounts.9b00053

Byrappa, K., & Adschiri, T. (2007). *Hydrothermal technology for nanotechnology*. *53*. Retrieved from https://doi.org/10.1016/j.pcrysgrow.2007.04.001

Chen, C., Hsu, C., Lai, S., Syu, W., Wang, T., & Lai, P. (2014). *Metal nanobullets for multidrug resistant bacteria and bio films ☆*. *78*, 88–104.

Dizaj, S. M., Barzegar-jalali, M., Zarrintan, M. H., Adibkia, K., & Lotfipour, F. (2015). *Calcium carbonate nanoparticles as cancer drug delivery system*. 1–12. Retrieved from https://doi.org/10.1517/17425247.2015.1049530

Dorati, R., Detrizio, A., Spalla, M., Migliavacca, R., Pagani, L., Pisani, S., Chiesa, E., . . . Genta, I. (2018). *Gentamicin sulfate PEG-PLGA / PLGA-H nanoparticles: Screening design and antimicrobial effect evaluation toward clinic bacterial isolates*. Retrieved from https://doi.org/10.3390/nano8010037

Fanny Chiat Orou, S., Hang, K. J., Thuya Thien, M., Ying, Y. L., Foh, L. C., Duong Ngoc Diem, N., . . . Pung, Y. F. (2018). Antibacterial activity by ZnO nanorods and ZnO nanodisks: A model used to illustrate "Nanotoxicity Threshold." *Journal of Industrial and Engineering Chemistry*, *62*(2017), 333–340. Retrieved from https://doi.org/10.1016/j.jiec.2018.01.013

Feng, W., Nie, W., Cheng, Y., Zhou, X., Chen, L., Qiu, K., . . . He, C. (2015). In vitro and in vivo toxicity studies of copper sulfide nanoplates for potential photothermal applications. *Nanomedicine: Nano technology, Biology, and Medicine*, *11*(4), 901–912. Retrieved from https://doi.org/10.1016/j.nano.2014.12.015

Goel, S., Chen, F., & Cai, W. (2014). Synthesis and biomedical applications of copper sulfide nanoparticles: from sensors to theranostics. *Small (Weinheim an Der Bergstrasse, Germany)*, *10*(4), 631–645. Retrieved from https://doi.org/10.1002/smll.201301174

Guilger, M., Pasquoto-Stigliani, T., Bilesky-Jose, N., Grillo, R., Abhilash, P. C., Fraceto, L. F., & De Lima, R. (2017). Biogenic silver nanoparticles based on trichoderma harzianum: Synthesis, characterization, toxicity evaluation and biological activity. *Scientific Reports*, *7*(October 2016), 1–13. Retrieved from https://doi.org/10.1038/srep44421

Imbuluzqueta, E., Gamazo, C., Lana, H., Campanero, M. Á., Salas, D., Gil, A. G., . . . Blanco-Prieto, M. J. (2013). Hydrophobic gentamicin-loaded nano particles are effective against Brucella melitensis infection in mice. *Antimicrobial Agents and Chemotherapy*, *57*(7), 3326–3333. Retrieved from https://doi.org/10.1128/AAC.00378-13

Junejo, Y., Safdar, M., Akhtar, M. A., Saravanan, M., Anwar, H., Babar, M., . . . Babar, M. E. (2019). Synthesis of tobramycin stabilized silver nanoparticles and its catalytic and antibacterial activity against pathogenic bacteria. *Journal of Inorganic and Organometallic Polymers and Materials*, *29*(1), 111–120. Retrieved from https://doi.org/10.1007/s10904-018-0971-z

Kanagamani, K., Muthukrishnan, P., Shankar, K., Kathiresan, A., Barabadi, H., & Saravanan, M. (2019). Antimicrobial, cytotoxicity and photocatalytic degradation of norfloxacin using kleinia grandiflora mediated silver nanoparticles. *Journal of Cluster Science*, *30*(6), 1415–1424. Retrieved from https://doi.org/10.1007/s10876-019-01583-y

Kotian, S. Y., Abishad, P. M., Byrappa, K., & Rai, K. M. L. (2019). Potassium iodate (KIO 3) as a novel reagent for the synthesis of isoxazolines: evaluation of

antimicrobial activity of the products. *Journal of Chemical Sciences*, *131*(6), 1–6. Retrieved from https://doi.org/10.1007/s12039-019-1622-9

Luthra, S., Rominski, A., & Sander, P. (2018). The role of antibiotic-target-modifying and antibiotic-modifying enzymes in mycobacterium abscessus drug resistance. *Frontiers in Microbiology*, *9* (September), 1–13. Retrieved from https://doi.org/10.3389/fmicb.2018.02179

Maleki Dizaj, S., Lotfipour, F., Barzegar-Jalali, M., Zarrintan, M. H., & Adibkia, K. (2016). Physicochemical characterization and antimicrobial evaluation of gentamicin-loaded CaCO3nanoparticles prepared via microemulsion method. *Journal of Drug Delivery Science and Technology*, *35*, 16–23. Retrieved from https://doi.org/10.1016/j.jddst.2016.05.004

Mofokeng, T. P., Moloto, M. J., Shumbula, P. M., & Tetyana, P. (2019). Synthesis, characterization and cytotoxicity of alanine-capped CuS nanoparticles using human cervical carcinoma HeLa cells. *Analytical Biochemistry*, *580*(April), 36–41. Retrieved from https://doi.org/10.1016/j.ab.2019.06.008

Mosmann, T. (1983). Rapid colorimetric assay for cellular growth and survival: Application to proliferation and cytotoxicity assays. *Journal of Immunological Methods*, *65*(1–2), 55–63. Retrieved from https://doi.org/10.1016/0022-1759(83)90303-4

Mukherjee, P., Ahmad, A., Mandal, D., Senapati, S., Sainkar, S. R., Khan, M. I., . . . Sastry, M. (2001). Fungus-mediated synthesis of silver nanoparticles and their immobilization in the mycelial matrix: A novel biological approach to nanoparticle synthesis. *Nano Letters*, *1*(10), 515–519. Retrieved from https://doi.org/10.1021/nl0155274

Mukhopadhyay, D., & Sarkar, G. (2006). *The use of microorganisms for the formation of metal nanoparticles and their application*. 485–492. Retrieved from https://doi.org/10.1007/s00253-005-0179-3

Neelgund, G. M., Oki, A., Bandara, S., & Carson, L. (2021). Photothermal effect and cytotoxicity of CuS nanoflowers deposited over folic acid conjugated nanographene oxide. *Journal of Materials Chemistry B*, *9*(7), 1792–1803. Retrieved from https://doi.org/10.1039/d0tb02366c

Ottoni, C. A., Simões, M. F., Fernandes, S., dos Santos, J. G., da Silva, E. S., de Souza, R. F. B., & Maiorano, A. E. (2017). Screening of filamentous fungi for antimicrobial silver nanoparticles synthesis. *AMB Express*, *7*(1). Retrieved from https://doi.org/10.1186/s13568-017-0332-2

Pajerski, W., Ochonska, D., Brzychczy-Wloch, M., Indyka, P., Jarosz, M., Golda-Cepa, M., Sojka, Z., & Kotarba, A. (2019). Attachment efficiency of gold nanoparticles by Gram-positive and Gram-negative bacterial strains governed by surface charges. *Journal of Nanoparticle Research*, *21*(8). Retrieved from https://doi.org/10.1007/s11051-019-4617-z

Papich, M. G. (2016). Gentamicin Sulfate. *Saunders Handbook of Veterinary Drugs*, 353–355. Retrieved from https://doi.org/10.1016/b978-0-323-24485-5.00280-1

Pugazhendhi, A., Kumar, S. S., Manikandan, M., & Saravanan, M. (2018). Photocatalytic properties and antimicrobial efficacy of Fe doped CuO nanoparticles against the pathogenic bacteria and fungi. *Microbial Pathogenesis*, *122*(June), 84–89. Retrieved from https://doi.org/10.1016/j.micpath.2018.06.016

Qi, J., Wen, J., Wang, Q., Jin, X., & Zhou, X. (2020). Preparation and photocatalytic properties of hexagonal and orthogonal CuS micro-nanoparticles by an oil-water interface method. *Materials Chemistry and Physics*, *255*(August), 123629. Retrieved from https://doi.org/10.1016/j.matchemphys.2020.123629

Saranya, M., Santhosh, C., Ramachandran, R., & Nirmala Grace, A. (2014). Growth of CuS nanostructures by hydrothermal route and its optical properties. *Journal of Nanotechnology*, *2014*. Retrieved from https://doi.org/10.1155/2014/321571

Solanki, J. N., Sengupta, R., & Murthy, Z. V. P. (2010). Synthesis of copper sulphide and copper nanoparticles with microemulsion method. *Solid State Sciences*, *12*(9), 1560–1566. Retrieved from https://doi.org/10.1016/j.solidstatesciences.2010.06.021

Van Tonder, A., Joubert, A. M., & Cromarty, A. D. (2015). Limitations of the 3-(4,5-dimethylthiazol-2-yl)-2,5-diphenyl-2H-tetrazolium bromide (MTT) assay when compared to three commonly used cell enumeration assays. *BMC Research Notes*, *8*(1), 1–10. Retrieved from https://doi.org/10.1186/s13104-015-1000-8

Wang, C., Kim, Y. J., Singh, P., Mathiyalagan, R., Jin, Y., & Yang, D. C. (2016). Green synthesis of silver nanoparticles by Bacillus methylotrophicus, and their antimicrobial activity. *Artificial Cells, Nanomedicine and Biotechnology*. Retrieved from https://doi.org/10.3109/21691401.2015.1011805

Wang, Y., Jiang, F., Chen, J., Sun, X., Xian, T., & Yang, H. (2020). In situ construction of CNT/cus hybrids and their application in photodegradation for removing organic dyes. *Nanomaterials*, *10*(1). Retrieved from https://doi.org/10.3390/nano10010178

Zare, M., Namratha, K., Byrappa, K., Surendra, D. M., Yallappa, S., & Hungund, B. (2018). Surfactant assisted solvothermal synthesis of ZnO nanoparticles and study of their antimicrobial and antioxidant properties. *Journal of Materials Science and Technology*, *34*(6), 1035–1043. Retrieved from https://doi.org/10.1016/j.jmst.2017.09.014